www.czasopisma.pan.pl PAN POLSKA AKADEMIA NAUK www.journals.pan.pl

Arch. Metall. Mater. **64** (2019), 2, 571-578

DOI: 10.24425/amm.2019.127580

IM DOO JUNG*, JUNGHO CHOE*†, JAECHEOL YUN*, SANGSUN YANG*,
DONG-YEOL YANG*, YONG-JIN KIM*, JI-HUN YU*#

DUAL SPEED LASER RE-MELTING FOR HIGH DENSIFICATION IN H13 TOOL STEEL METAL 3D PRINTING

The densification behavior of H13 tool steel powder by dual speed laser scanning strategy have been characterized for selective laser melting process, one of powder bed fusion based metal 3d printing. Under limited given laser power, the laser re-melting increases the relative density and hardness of H13 tool steel with closing pores. The single melt-pool analysis shows that the pores are located on top area of melt pool when the scanning speed is over 400 mm/s while the low scanning speed of 200 mm/s generates pores beneath the melt pool in the form of keyhole mode with the high energy input from the laser. With the second laser scanning, the pores on top area of melt pools are efficiently closed with proper dual combination of scan speed. However pores located beneath the melt pools could not be removed by second laser scanning. When each layer of 3d printing are re-melted, the relative density and hardness are improved for most dual combination of scanning. Among the scan speed combination, the 600 mm/s by 400 mm/s leads to the highest relative density, 99.94 % with hardness of 53.5 HRC. This densification characterization with H13 tool steel laser re-melting can be efficiently applied for tool steel component manufacturing via metal 3d printing.

Keywords: Metal 3d printing, Powder bed fusion, Selective laser melting, H13 tool steel, re-melting

1. Introduction

H13 is a hot-work steel widely used in die casting, hot forging, injection molding [1,2]. Due to its high toughness, hardness and wear resistance property, complex shape design of H13 steel is hard with conventional fabrication method such as casting and forging and excessive time and cost can be required for H13 component design customization. In this regard, metal 3d printing, also known as metal additive manufacturing (AM) method has been recently used to build up a complex shape H13 components [3,4]. Metal AM method uses metal powders and laser sintering/melting to build up a three dimensional parts. With the principle of layer-by-layer additive process, this process has high degree of freedom for shaping. Selective laser melting (SLM) is one of metal AM process using powder bed fusion principle which is able to develop higher accuracy fabrication than the other AM process such as direct energy deposition (DED) method [5,6]. With this benefit of SLM, complicated shape of mold steel component can be developed. For example, unique design of conformal cooling channel or cavity can be made with SLM [7].

Despite of these benefits, there still exists various problems to overcome in SLM such as low relative density and low mechanical property [8-10]. There have been several studies to increase relative density by SLM by control laser power and scan speed for H13 tool steel [11,12]. Post process of hot isostatic pressing (HIP) method are used to increase density after printing [13,14]. However, HIP process requires much time and cost additionally. In this regards, laser re-melting or re-scanning method have been applied to obtain high densification during SLM process [15-17] which was normally applied only on the surface of metal component to obtain fine surface finishing [18-21]. Laser re-melting during SLM process can increase the density by closing pores in each layers. However, improper re-melting strategies can results in reverse effect on densification.

In this study, we aim to develop dual scan speed combination process for laser re-melting to obtain high density of H13 components via SLM. The laser was exposed twice on the same surface of pattern in each layer during SLM process. The scan speed of first exposure and second exposure were changed to match the optimum combination for closing pores. Printed specimens with each combination of scan speeds were compared to verify optimum process condition.

2. Materials and experimental procedure

Commercial H13 powder (Sandvik Co.) was used for SLM process. Fig. 1 shows the morphology and particle size distribution of H13 powder used in this study. As shown in Fig. 1(a), powder has spherical shape with a few satellites on the surface. This spherical shape of powder is important for uniform coating of each layer in SLM. Fig. 1(b) shows the particle size distribu-

* 3D PRINTING MATERIALS CENTER, KOREA INSTITUTE OF MATERIALS SCIENCE, 797 CHANGWON-DAERO, JUNGANG-DONG, SEONGSAN-GU, CHANWON-SI, GYEONGSANGNAM-DO, SOUTH KOREA

† Equally contributed as first author

Corresponding authors: jhyu01@kims.re.kr; idjung84@kims.re.kr

tion measured by laser diffraction method. The D50 particle size was 35 mm and the standard deviation was 4.6. This narrow size distribution can enhance the flowability during re-coating in SLM [22]. The flow rate was measured by hall flow meter with ASTM B213 and it showed 16.7 sec/50g.

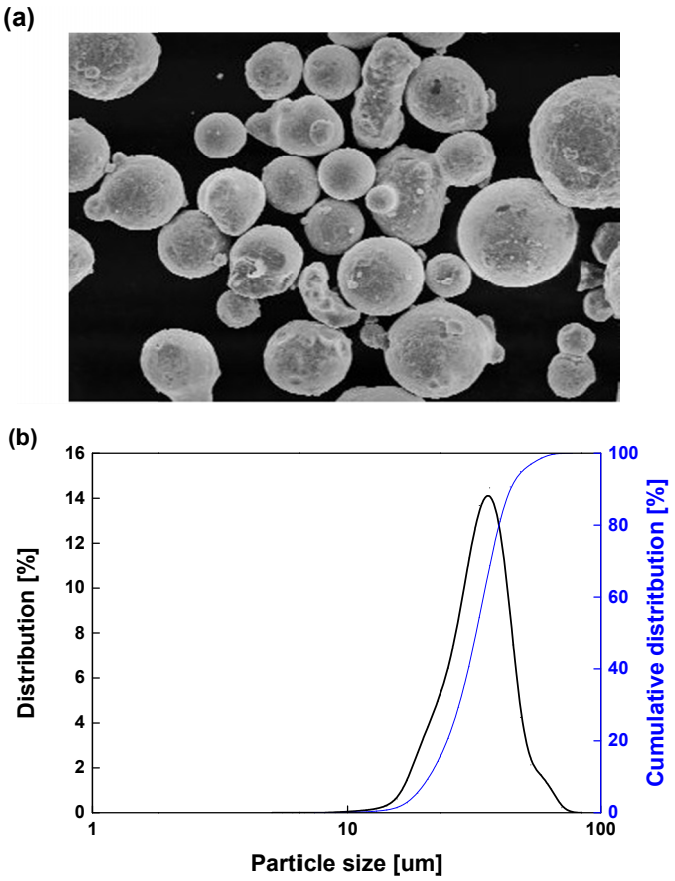

Fig. 1. Characterization of H13 powder. (a) SEM Morphology of H13 Powder (Scale bar: 20 mm), (b) Laser diffraction analysis of particle size distribution

For SLM process, M. LAB (Concept Laser Co.) was employed, which uses powder bed fusion principle for metal 3d printing. The oxygen level during printing was maintained below 0.3% with argon as atmosphere gas. To compare the dual scan speed combination of laser re-melting, the laser power, hatch space and single layer thickness were fixed at 90 W, 80 mm and 25 mm respectively. The first and second scan speed was varied within 100 mm/s~1000 mm/s. To observe pore formation in single melt pool during general re-melting process, same speed combination of first and second scan was conducted in single line printing with H13 powder on stainless 316L plate. To compare the density and mechanical hardness with dual scan speed re-melting, cubic shape (1cm x1cm x1cm) H13 components were printed by dual scan planning. The percentage of pores were calculated from the cross-sectional optical microscopy images via image analysis and Rockwell C hardness test was conducted to measure hardness of H13 printed components.

3. Results and discussion

Fig. 3 shows the single melt pool cut surface morphology of single scanning with 200 mm/s, 400 mm/s, 600 mm/s and 800 mm/s. As shown in Fig. 3(a), there existed pores at the beneath of large melt pool, which is a key hole mode generated by too high laser energy given to H13 powders and evaporation of metal [23,24]. This keyhole mode is one of factor that limit the volumetric energy density according to laser scan speed and power as a design parameter in SLM [25]. Too slow scan speed in Fig. 3(a) resulted in relatively high input energy into melt pool which led to this defect. Fig. 3(b) shows the single melt pool morphology with scan speed of 400 mm/s. The melt pool size of (b) is much smaller than (a) and there existed multiple pores in the single melt pool. As show in Fig. 3(c), the single melt pool of 600 mm/s is slightly smaller than (b) and reduced number and size of pores exist near the top surface of melt pool. Fig. 3(d) shows the single melt pool of 800 mm/s which is the smallest in size among four scan speeds.

Figs. 4~7 shows the single melt pool cut surface morphology with laser re-melting of different combination of scan speeds. Fig. 4 shows the single melt pool cut surface processed by dual scan speeds ((a) 200 mm/s followed by 200 mm/s, (b) 200 mm/s followed by 400 mm/s, (c) 200 mm/s followed by 600 mm/s and (d) 200 mm/s followed by 800 mm/s). All four

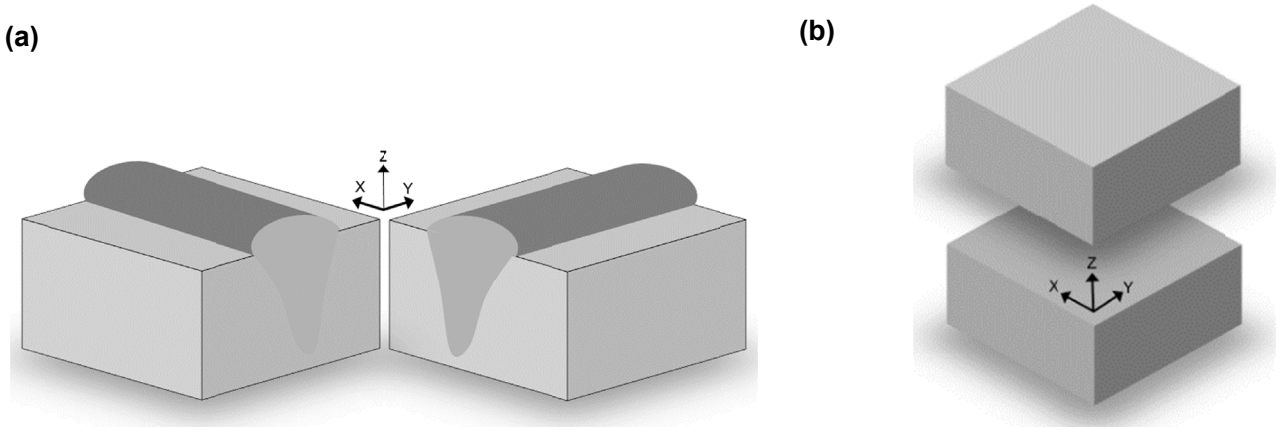

Fig. 2. Schematic diagram of H13 SLM component. (a) Single melt pool analysis, (b) Cubic (1 cm×1 cm×1 cm) specimen analysis

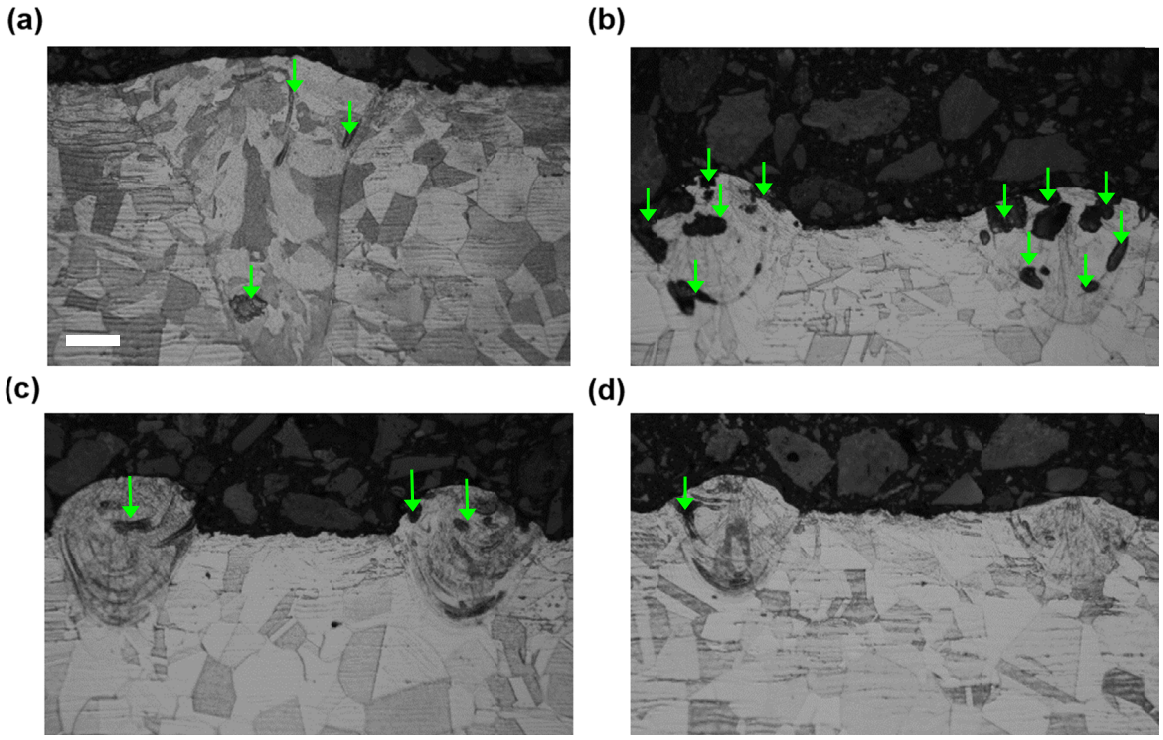

Fig. 3. Single melt pool analysis of 1 time scanning (a) 200 mm/s, (b) 400 mm/s, (c) 600 mm/s, (d) 800 mm/s (Scale bar : 70 mm)

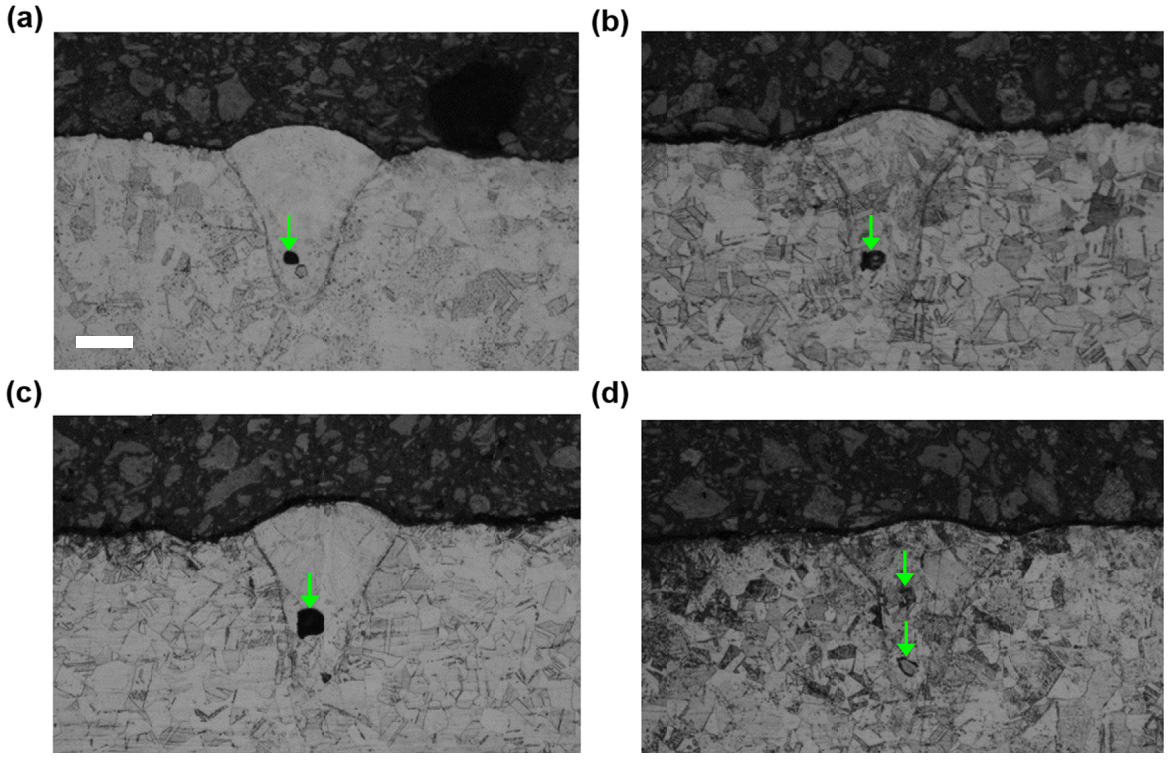

Fig. 4. Single melt pool analysis of dual scanning with first speed of 200 mm/s (a) Second speed 200 mm/s, (b) Second speed 400 mm/s, (c) Second speed 600 mm/s, (d) Second speed 800 mm/s (Scale bar : 70 mm)

specimens had key holes near the bottom of melt pool. This existence of keyhole mode indicates that the second melting could not remove the defect located bottom of the melt pool. With the first scan speed of 200 mm/s, the re-melting with different combination of second scan speeds (200 mm/s~800 mm/s) could not remove the key holes which are located too deep in the melt pool generated by first low scan speed 200 mm/s with high energy density.

The single melt pool with first scan speed of 400 mm/s and second scan speed from 200 mm/s to 800 mm/s are shown in Fig. 5. The single melt pool of 400 mm/s followed by 200 mm/s had key hole near the bottom area while the others didn't have

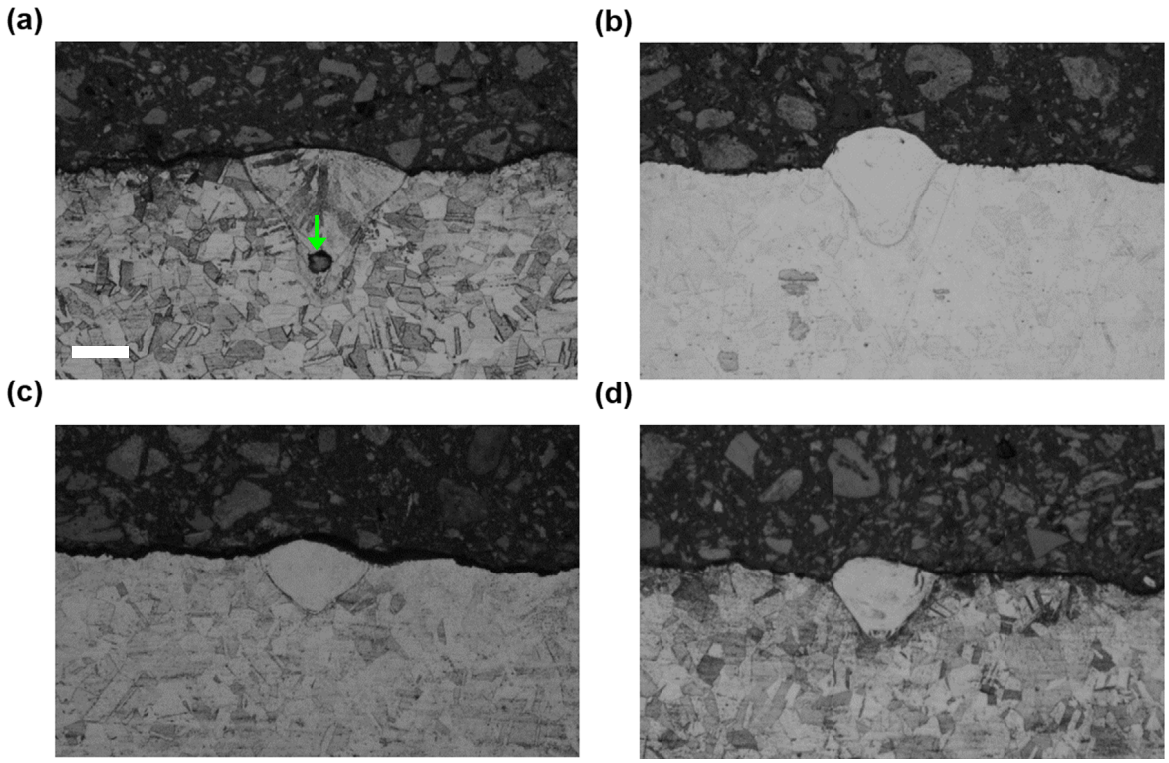

Fig. 5. Single melt pool analysis of dual scanning with first speed of 400 mm/s (a) Second speed 200 mm/s, (b) Second speed 400 mm/s, (c) Second speed 600 mm/s, (d) Second speed 800 mm/s (Scale bar : 70 mm)

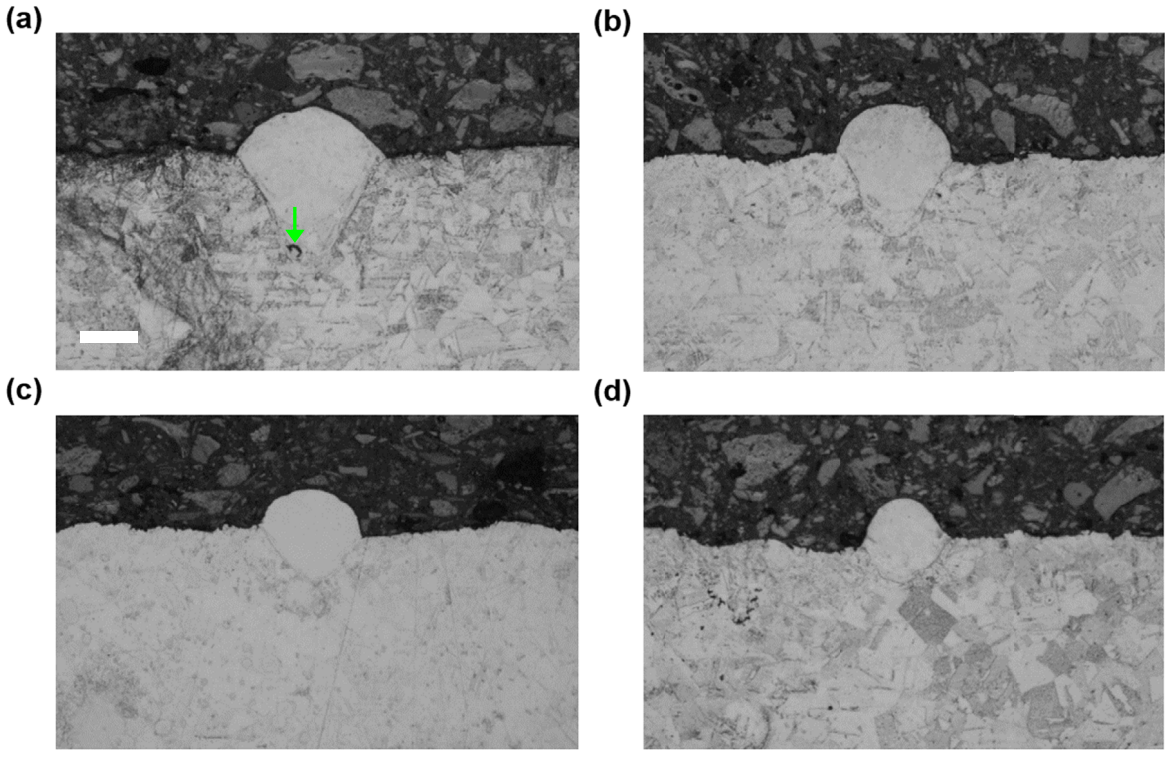

Fig. 6. Single melt pool analysis of dual scanning with first speed of 600 mm/s (a) Second speed 200 mm/s, (b) Second speed 400 mm/s, (c) Second speed 600 mm/s, (d) Second speed 800 mm/s (Scale bar : 70 mm)

such defects. The width and dept of the single melt pool decreased as the second re-melting scan speed increased. The melt pool size of second scan speed 800 mm/s was anout 1/4 times smaller than that of 200 mm/s. Fig. 6 shows the single melt pool with first scan speed of 600 mm/s and its combination with second scan speed from 200 mm/s to 800 mm/s. The key hole in 600 mm/s followed by 200 mm/s was much smaller than that of 200 mm/s followed by 600 mm/s and 400 mm/s followed

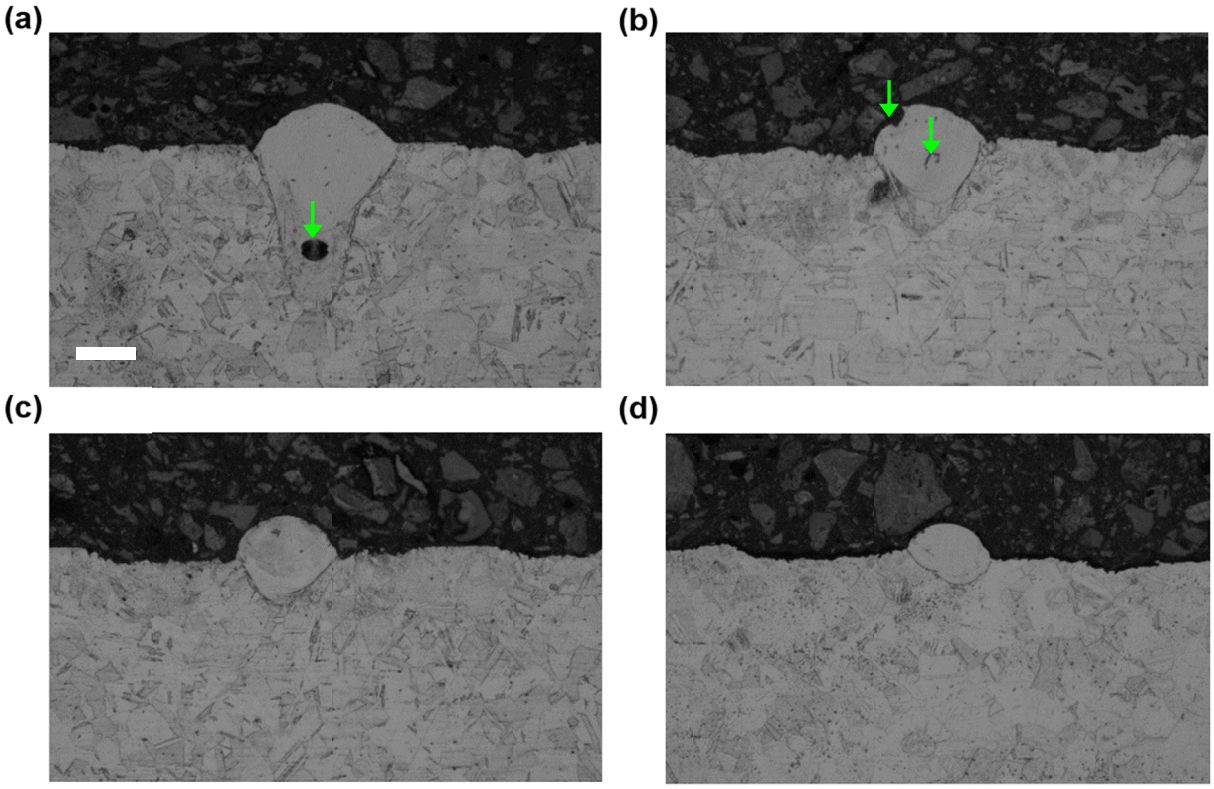

Fig. 7. Single melt pool analysis of dual scanning with first speed of 800 mm/s (a) Second speed 200 mm/s, (b) Second speed 400 mm/s, (c) Second speed 600 mm/s, (d) Second speed 800 mm/s (Scale bar : 70 mm)

by 200 mm/s as shown in Fig. 6(a). For 600 mm/s followed by 400 mm/s, 600 mm/s or 800 mm/s, no significant defects were observed while the size of melt pool decreased as second scan speed increased.

The single melt pool with first scan speed of 800 mm/s and its combination with second scan speed from 200 mm/s to 800 mm/s are shown in Fig. 7. Similarly with Figs. 5 and 6, the combination with second scan speed 200 mm/s led to key hole near the bottom of large melt pool. The overall melt pool size of four specimen was the smallest among other first scan speed from 200 mm/s to 600 mm/s. As shown in Fig. 7(d), the melt pool was almost 20 % of Fig. 7(a) in size. The optical image of 3d printed H13 cut-surface with different dual scan strategy was summarized in Fig. 8. With first scan speed of 200 mm/s, no significant improvement was induced by the re-melting with second scan speed ranging from 200 mm/s to 800 mm/s. According to the single melt pool analysis in Figs. 3~7, this unaffecting re-melting effect could be caused by the key holes located near the bottom of melt pool which cannot be easily removed by the second melting. Dual speed re-melting combination with first scan speed 200 mm/s could not recover the generated pores. With 400 mm/s of first laser scanning, pores were reduced with re-melting of second scan speed ranging from 400 mm/s to 800 mm/s. The too law speed in second scanning of 200 mm/s led to generation of pores due to its high energy density causing key hold mode while too high speed in second scanning of 800 mm/s or 1000 mm/s could not close the pores. Cracks were observed in the specimen of 400 mm/s by 1000 mm/s. With the comparision with single melt pool analysis in Figs. 3 and 5, too small melt pool size with high scan speed could induce not enough overlapping of melt pool related such crack defect. The scan speed combination of 400 mm/s followed by 600 mm/s led to the least existence of pores.

With 600 mm/s of first laser scanning, 400 mm/s and 600 mm/s resulted in most reduction of pores by re-melting. However, specimen with 600 mm/s followed by 600 mm/s had regional big pores which could cause degradation of mechanical property. For 800 mm/s and 1000 mm/s, more percentage of larger pores appeared which could reduce the relative density and mechanical property. According to the single melt pool analysis of dual scan speed scanning in Figs. 3 and 6, too small melt pool size with fast speed of first and second scanning could induce such defects. With 800 mm/s of first laser scanning, most specimen had large number of small pores or large size pores or nannow line cracks connecting pores.

In Fig. 9, the characteristic densification behavior in each combination of dual speed re-melting is quantitatively analyzed with image analysis of generated pores. Fig. 9(a) shows the calculated number of pores per square centimeter in each specimen with different dual scan speed. For specimen with first scan speed of 200 mm/s, the re-melting with 100 mm/s~1000 mm/s increased the number of pores which mean that re-melting had reversal effect for densification with such low first scan speed. In addition, the number of pores with second scan speed above 400 mm/s were decreased by more than 50% than with the second scan speed of 200 mm/s. Over 400 mm/s of second scan

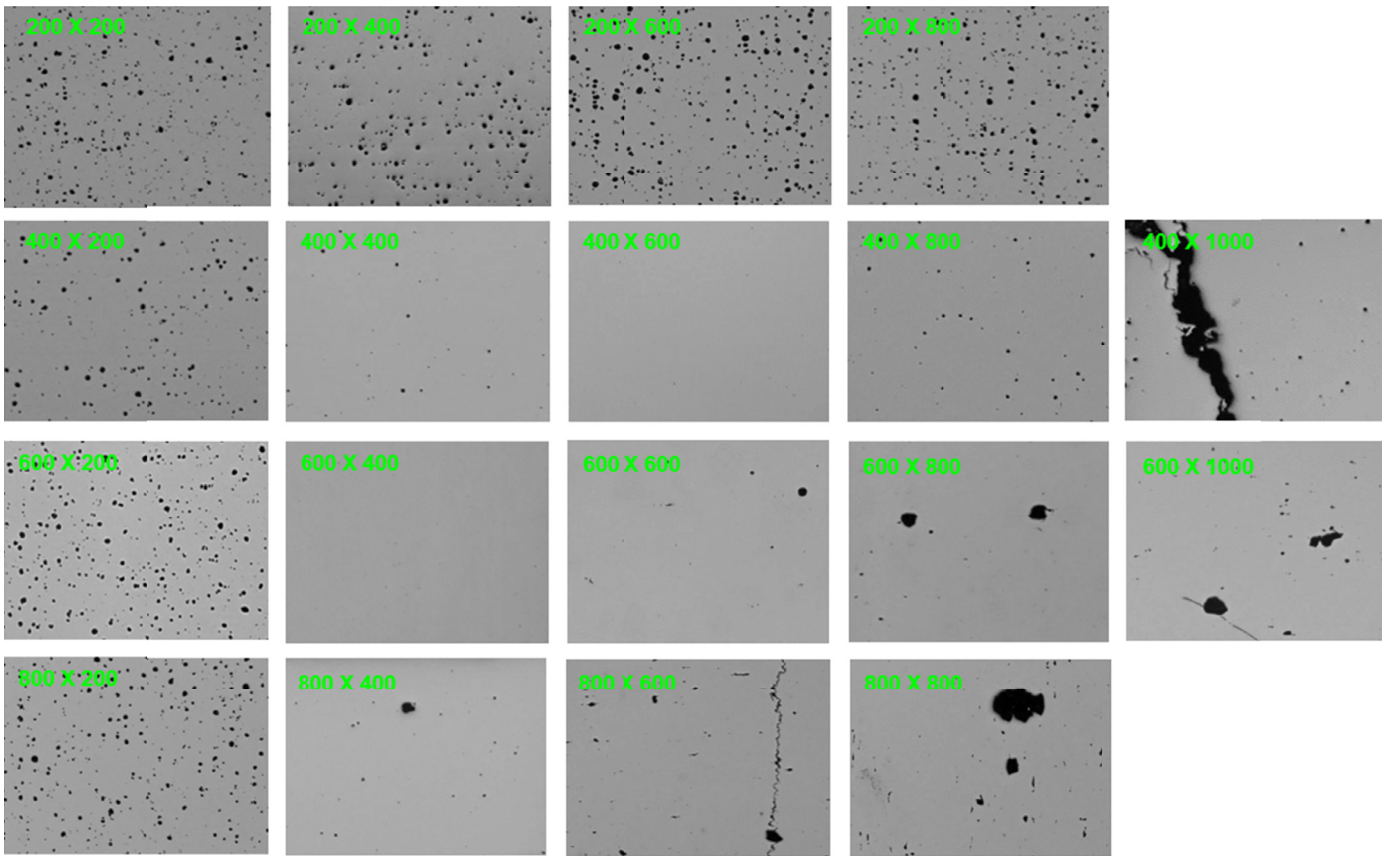

Fig. 8. Laser Re-melting specimen optical image with different combination of scan speed (Scale bar : 400 mm)

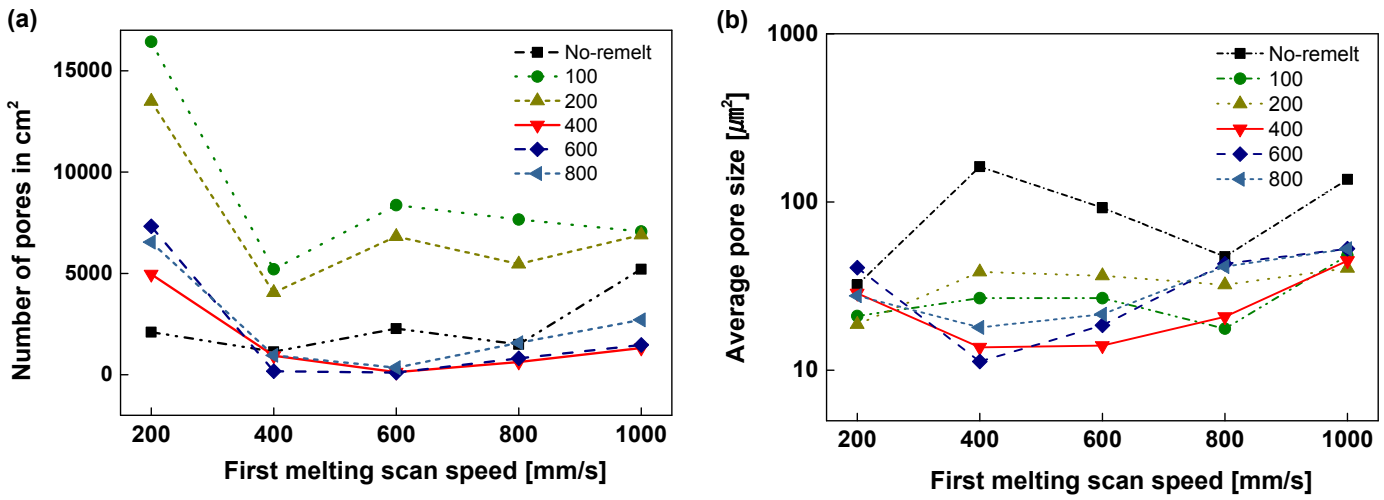

Fig. 9. Image analysis of generated pore characterization (a) Number of pores in square centimeter, (b) Average pore size

speed, there existed clear reduction of pores under re-melting with second scan speed above 400 mm/s. For the first scan speed 400 mm/s, the overall number of pores were about 55% of the specimens with first scan speed 200 mm/s. The dual combination with 400 mm/s followed by 600 mm/s dramatically reduced the number of pores almost close to zero while there was no significant change in combination with the other second scan speed (800 mm/s, 1000 mm/s). Similarly, for first scanning with 600 mm/s, second scan speed over 400 mm/s showed 75% reduction of pores compared to second scan speed of 200 mm/s. Regardless of first scan speed, the pores generally increased by higher second speed above 400 mm/s. Fig. 9 (b) shows the average size of pores in each combination of scan speeds. The average pore size of first scan speed, 1000 mm/s was higher than the other first speed of scanning and first scan speed of 400 mm/s and 600 mm/s had the lowest average size of pores.

The hardness and relative density of printed metal specimens were summarized in Fig. 10. The single scan 3D printing of H13 had relative density ranging from 95% to 98% with scan speeds ranging from 200mm/s to 800 mm/s. The hardness of

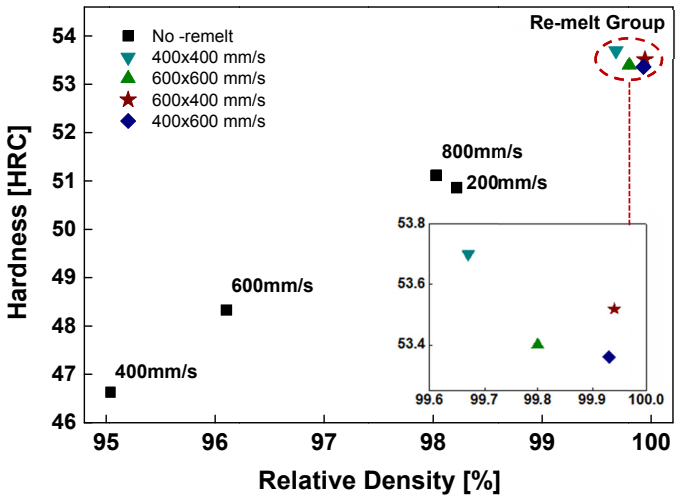

Fig. 10. The hardness and relative density of 3D printed H13 specimen

single scan 3D printing was in between 46 and 52 HRC. While the relative density and hardness of single 3D printing with scan speed 400 mm/s and 600 mm/s were relatively lower than that of 200 mm/s and 800 mm/s, most positive re-melting effect were obtained appeared with first scan speed of 400 mm/s and 600 mm/s which had relative density over 99.5% and hardness over 53 HRC. Among the re-melted specimens, the specimen with 600 by 400 mm/s showed nearly full density of 99.94% with high hardness 53.5 HRC.

4. Conclusion

H13 tool steel have been printed by selective laser melting with different laser scan plan and characterized by relative density and hardness. The re-melting of H13 tool steel increased the relative density and hardness with closing pores generated by first single laser scanning. Too low first laser scanning of 200 mm/s led to key hole defects beneath the melt pool, which could not be efficiently removed by second melting with scanning speed from 200 mm/s to 800 mm/s. The pores were generated on top area of melt pool with first scanning of 400 mm/~800 mm/s and they were successfully removed by second laser scanning. Nearly full density of 99.94% was achived for H13 tool steel by metal 3D printing based on SLM. These results can be very useful to fabricate H13 tool steel by selective laser melting process with understanding of characteristic densification behavior under different combination of first and second laser melting.

Acknowledgement

This study was supported financially by Fundamental Research Program "Development of High Performance Materials and Processes for Metal 3D Printing (PNK6050)" of the Korean Institute of Materials Science (KIMS).

REFERENCES

[1] M. Kang, G. Park, J. G. Jung, B.H. Kim, Y.K. Lee, The effects of annealing temperature and cooling rate on carbide precipitation behavior in H13 hot-work tool steel, Journal of Alloys and Compounds **627**, 359-366 (2015),

[2] J.Y. Li, Y.L. Chen, J.H. Huo, Mechanism of improvement on strength and toughness of H13 die steel by nitrogen, Materials Science and Engineering: A **640**, 16-23 (2015).

[3] J. Krell, A. Rottger, K. Ggeenen, W. Theisen, General investigations on processing tool steel X40CrMoV5-1 with selective laser melting, Journal of Materials Processing Tech. **255**, 679-688 (2018).

[4] F. Deirmina, B. Mangour, D. Grzesiak, M. Pellizzari, H13-partially stabilized zirconia nanocomposites fabricated by high-energy mechanical milling and selective laser melting, Materials and Design **146**, 286-297 (2018).

[5] S. Bremen, W. Meiners, A. Diatlov, Selective laser melting, Laser Technik Journal **9**, 33-38 (2012).

[6] C. Y. Yap et al., Review of selective laser melting: Materials and applications, Applied Physics Reviews **2**, 4 (2015).

[7] A. Armillotta, R. Baraggi, S. Fasoli, SLM tooling for dies casting with conformal cooling channels, International Journal of Advanced Manufacturing Technology **71**, 573-583 (2014).

[8] S.A. Khairallah, A.T. Anderson, A. Rubenchik, W.E. King, Laser powder-bed fusion additive manufacturing: Physics of complex melt flow and formation mechanisms of pores, spatter, and denudation zones, Acta Materialia **108**, 36-45 (2016).

[9] C. Qiu, C. Panwisawas, M. Ward, H.C. Basoalto, J.W. Brroks, M.M. Attallah, On the role of melt flow into the surface structure and porosity development during selective laser melting, Acta Materialia **96**, 72-79 (2015).

[10] G. Tapia, A.H. Elwany, H. Sang, Prediction of porosity in metal-based additive manufacturing using spatial Gaussian process models, Additive Manufacturing **12**, 282-290 (2016).

[11] P. Laakso, T. Riipinen, A. Laukkanen, T. Andersson, A. Jokinen, A. Revuelta, K. Ruusuvuori, Optimization and simulation of SLM process for high density H13 tool steel parts, Physics Procedia **83**, 26-35 (2016).

[12] T.H.C. Childs, C. Hauser, M. Badrossamary, Selective laser sintering (melting) of stainless and tool steel powders: experiments and modelling, Proceedings of the Institution of Mechanical Engineers, Part B: Journal of Engineering Manufacture **219**, 339-357 (2005).

[13] S. Das, M. Wohlert, J.J. Beaman, D.L. Bourell, The journal of the materials, metals & materials society (TMS) **50**, 17-20 (1998).

[14] S.T. Williams, P.J. Withers, I. Todd, P.D. Prangnell, The Effectiveness of Hot Isostatic Pressing for Closing Porosity in Titanium Parts Manufactured by Selective Electron Beam Melting, Metallurgical and Materials Transactions A **47**, 1939-1946 (2016).

[15] T. Hwang, Y.Y. Woo, S.W. Han, Y.H. Moon, Functionally graded properties in directed-energy-deposition titanium parts, Optics and Laser Technology **105**, 80-88 (2018).

[16] M. Hirsch et. al., Targeted rework strategies for powder bed additive manufacture, Additive Manufacturing **19**, 127-133 (2018).

[17] E. Yasa, J. Kruth, Application of laser re-melting on selective laser melting parts, Advances in Production Engineering & Management **6**, 259-270 (2011).

[18] E. Kayahan, A post-processing study on aluminum surface by fiber laser: Removing face milling patterns, Optics and Laser Technology **101**, 440-445 (2018).

[19] S. Zhou et. al., Effect of laser remelting on microstructure and properties of WC reinforced Fe-based amorphous composite coatings by laser cladding, Optics and Laser Technology **103**, 8-16 (2018).

[20] J. Vaithilingam, R.D. Goodrige, R.J.M. Hauge, S.D.R. Christie, S. Edmondson, The effect of laser remelting on the surface chemistry of Ti6al4Vcomponents fabricated by selective laser melting, Journal of Materials Processing Technology **232**, 1-8 (2016).

[21] T.F. Flint, C. Panwisawas, Y. Sovani, M.C. Smith, H.C. Basoalto, Prediction of grain structure evolution during rapid solidification of high energy density beam induced re-melting, Materials and Design **147**, 200-210 (2018).

[22] I. Yadroitsev, P. Bertrand, I. Smurov, Parametric analysis of the selective laser melting process, Applied surface science **253**, 8064-8069 (2007).

[23] W.E. King et al., Observation of keyhole-mode laser melting in laser powder-bed fusion additive manufacturing, Journal of Materials Processing Technology **214**, 2915-2925 (2014).

[24] D. Dai, D. Gu, Effect of metal vaporization behavior on keyhole-mode surface morphology of selective laser melted composites using different protective atmospheres, Applied Surface Science **355**, 310-319 (2015).

[25] U.S. Bertoli, A.J. Wolfer, M.J. Matthews, J.P.R. Delplanque, J.M. Schoenung, On the limitations of Volumetric Energy Density as a design parameter for Selective Laser Melting, Materials & Design **113**, 331-340 (2017).